Process Biochemistry xxx (xxxx) xxx–xxx

Contents lists available at ScienceDirect

Process Biochemistry

journal homepage: www.elsevier.com/locate/procbio

Inhibition of *Zea mays* coniferyl aldehyde dehydrogenase by daidzin: A potential approach for the investigation of lignocellulose recalcitrance

Ana Paula Ferro[a], Rogério Flores Júnior[b], Aline Finger-Teixeira[a], Angela Valderrama Parizotto[a], Jennifer Munik Bevilaqua[a], Dyoni Matias de Oliveira[a], Hugo Bruno Correa Molinari[c], Rogério Marchiosi[a], Wanderley Dantas dos Santos[a], Flávio Augusto Vicente Seixas[b], Osvaldo Ferrarese-Filho[a,*]

[a] *Laboratory of Plant Biochemistry, Department of Biochemistry, University of Maringá, 87020-900, PR, Brazil*
[b] *Laboratory of Structural Biochemistry, Department of Biochemistry, University of Maringá, Umuarama, 87506-370, PR, Brazil*
[c] *Brazilian Agricultural Research Corporation, Division of Agroenergy, Brasília, 70770-917, DF, Brazil*

ARTICLE INFO

Keywords:
Lignocellulosic biomass
Maize
Homology modeling
Molecular dynamics
Saccharification
Virtual screening

ABSTRACT

Coniferyl aldehyde dehydrogenase (CALDH) catalyzes the oxidation of coniferyl aldehyde to ferulic acid. Because ferulic acid has a relevant role in the structure and recalcitrance of the cell wall, inhibition of CALDH can reduce its levels and increase the digestibility of lignocellulosic biomass. We prospected *in silico* a selective inhibitor of CALDH of *Zea mays*. The *Zmays*CALDH gene was identified by homology with the corresponding gene of *Arabidopsis thaliana*. The sequence was translated and analyzed, and the quaternary structure was modeled. A set of 20 putative inhibitors were screened from a virtual library and docked in the active site of *Zmays*CALDH, and daidzin (DZN) was selected as an enzyme inhibitor. The stability of the *Zmays*CALDH–DZN complex was evaluated by molecular dynamics simulations of the monomeric and tetrameric forms. For evaluation of kinetic analysis, *Zmays*CALDH activity was determined *in vitro* by high-performance liquid chromatography. In comparison to the DZN-free control, the data obtained indicated constant V_{max} and enhanced K_m. Altogether, *in silico* and *in vitro* findings indicated that DZN inhibited *Zmays*CALDH competitively. The DZN-induced inhibition of *Zmays*CALDH could be a valuable and promising approach to studies on ferulic acid biosynthesis and saccharification of lignocellulosic biomass.

1. Introduction

Today, the search for renewable and sustainable energy sources has become a major challenge due to the enhanced petroleum consumption associated with increased global greenhouse gas emissions, and the reduction of fossil feedstocks. In this scenario, lignocellulosic biomass is considered a non-toxic, abundant, cheap and energy-rich material for bioethanol production which can therefore reduce the current reliance on fossil fuel sources [1]. Lignocellulosic biomass consists of cellulose, hemicelluloses and lignin, which accounts for 20–30 % of the dry weight depending on the plant species [2]. Because it forms a physical barrier, lignin hinders the enzymatic degradation of cell-wall polysaccharides into monosaccharides followed by fermentation into ethanol, a process termed saccharification. Thus, to reduce this recalcitrance and to make polysaccharides more susceptible to hydrolytic enzymes is, now, the most prominent biotechnological challenge.

The type II cell walls of commelinoid monocots (*e.g.* grasses, sedges, rushes and gingers) are composed of a network of cellulose fibers encased in glucuronoarabinoxylans (GAX), low levels of pectin, structural proteins and elevated levels of hydroxycinnamates. An unusual feature of the primary and secondary cell walls of grasses is the presence of significant amounts of ferulic (up to 5 %) and *p*-coumaric (up to 3 %) acids [3]. As a metabolite of the phenylpropanoid pathway, ferulic acid has a preeminent role in the cell wall. It extensively dimerizes, forming cross-linkages between or within hemicelluloses and between hemicellulose and lignin [1,4]. That way, it can be ester-linked to arabinoxylans and ether-linked to lignins [5]. So, anchoring lignin in cell-wall polysaccharides contributes to cell-wall recalcitrance.

The complex cross-linkages between lignin and polysaccharides demand a set of enzymatic reactions to facilitate the access of polysaccharidases and release of fermentable sugars [6]. To date, the basic approaches to reduce cell-wall recalcitrance include manipulations of

* Corresponding author.
E-mail address: oferrarese@uem.br (O. Ferrarese-Filho).

https://doi.org/10.1016/j.procbio.2019.11.024
Received 8 May 2019; Received in revised form 21 October 2019; Accepted 20 November 2019

the biosynthetic pathway, quantity, composition and structure of lignin. In this way, challenging genetic engineering tools to reduce lignin content and alter its monomeric structure are one of main approaches [7]. Genetic manipulation of key enzymes of lignin biosynthesis has been extensively carried out with different plant species [8]. However, this can disturb other phenylpropanoid-derived pathways [9], affect cell-wall composition [10] and, in most cases, lead to unexpected effects on plant growth [11,12].

The phenylpropanoid pathway towards monolignol biosynthesis and, therefore, lignin is well characterized. However, discovery of new enzymes such as caffeoyl shikimate esterase (CSE), monolignol 4-*O*-methyltransferase (MOMT), monolignol ferulate transferase (MFT) and *p*-coumaroyl-CoA:monolignol transferase (PMT) [13–15] suggests new biosynthetic steps and branches of this traditional metabolic route. A new step to form ferulic acid from the phenylpropanoid pathway has been suggested in *Arabidopsis thaliana* [16]. Directly opposite to the traditional route, ferulic acid can be formed by the oxidation of coniferaldehyde and converted subsequently into feruloyl-CoA and linked to arabinoxylans and lignin. Isolation of the REF1 gene encoding a functional aldehyde dehydrogenase (ALDH) strengthens the likelihood that this metabolic step exists. Additionally, *in vitro* enzyme assays have detected coniferyl aldehyde dehydrogenase (CALDH, E.C.: 1.2.1.68) activity in maize (*Zea mays*); an indicative of the involvement of this enzyme in ferulic acid biosynthesis [16].

Specific enzyme inhibitors are finely tuned down-regulators of target enzymes and are therefore an essential tool for studying plant metabolism such as, for example, the phenylpropanoid pathway [17–19]. Due to the key role of *Z. mays* CALDH (*Zmays*CALDH) in ferulic acid synthesis, a specific inhibitor could be useful for studying the physiological role of this enzyme in plants. It could be used as a proof of concept to justify the development of *Z. mays* varieties with silencing of the CALDH gene, which could be extended to forage crops and for bioenergy applications. Moreover, it could be used as a useful alternative tool in genetically modified organisms in studies to reduce cell-wall recalcitrance, with applications for the food industry and biofuels.

Because ferulic acid has a relevant structural role, we hypothesized that inhibition of CALDH activity would open a new opportunity to control feruloylation [5], reduce recalcitrance and improve biomass digestibility. With this idea in mind, we resorted to bioinformatics to prospect potential inhibitors for this enzyme. We made this choice because bioinformatic tools allow prediction of the three-dimensional structure of non-crystallized enzymes by homology with similar crystallized proteins. The precision is enough for virtual screening of potential inhibitors by molecular docking. Once selected, the compounds may be quickly tested in *in vitro* or *in vivo* conditions.

For all the aforementioned reasons, it would be of interest to modeling the 3D structure of *Zmays*CALDH and to investigate *in silico* its putative inhibitors by using virtual screening and molecular docking techniques. These were the main objectives of the current work. Complementarily, and to corroborate the reliability of the structural model obtained *in silico*, *in vitro* kinetic analyses were done with daidzin (DZN, CID107971; Fig. 1), and the type of inhibition was determined.

2. Materials and methods

2.1. Experimental materials

Maize (*Zea mays* L. cv. IPR-114) seeds were obtained from Agronomic Institute of Paraná (Londrina, Brazil). Coniferyl aldehyde (≥98 %), ferulic acid (≥99 %), protease inhibitor cocktail (P9599), methanol (HPLC grade) and acetic acid (HPLC grade) were purchased from Sigma-Aldrich (St. Louis, MO, USA), and used without further purification. Ultrapure water was obtained by passage through Milli-Q purification system (Millipore, Molsheim, France). All other reagents used were of the purest grade available.

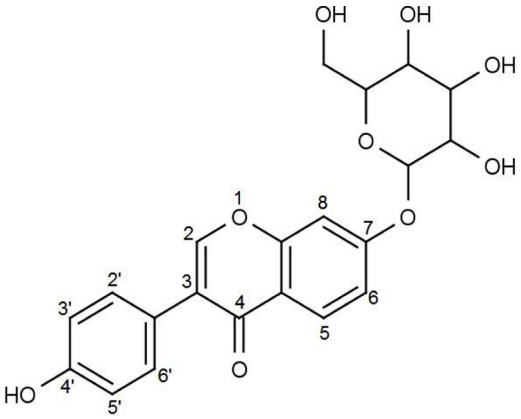

Fig. 1. Chemical structure of DZN. The portion isoflavone joined by an ether linkage between the C-7 and C-1 of glucose.

2.2. Identification of the amino acid sequence

The REF1 gene sequence (T43357) from *A. thaliana* [16] was used to search for *Zmays*CALDH homologous nucleotide sequences in the databases from the National Center for Biotechnology Information (NCBI), European Nucleotide Archive (ENA) and Plant Transcript Assemblies (TIGR), with accession number EU969650.1. This nucleotide sequence was translated into amino acids by Translate software and used to search the rating by the Basic Local Alignment Search Tool (BLAST) against the UniProt database [20]. Further, the resulting sequence of *Zmays*CALDH was analyzed to identify structural motifs *via* InterPro Scan, and prediction of physical-chemical parameters was done using the ProtParam tool [20,21].

2.3. Homology modeling

The search for structural templates was performed *via* BLASTp using *Zmays*CALDH sequences against the Protein Data Bank (PDB), and by fold recognition *via* pGenThreader [22]. The best templates selected in common by both tools were used as the input parameters for the program Modeller 9v10 [23]. A thousand structural models were generated from a single subunit, and the best model was chosen by Modeller dope score and validated *via* Procheck [24]. After the virtual screening steps, the tetrameric structure of CALDH (*Zmays*CALDHt) bonded to the best pose of the selected inhibitor was also modeled by geometric docking over each chain of the tetrameric form of the same template.

2.4. Virtual screening

The library of inhibitors was built by searching the databases PubChem, Drug Bank, Chembl, Zinc and Binding Database for substances with an inhibitory effect on human ALDH (alcohol deterrents) by using the purchasable filtering [25–29]. Then, the final *Zmays*-CALDH modeled structure was used for docking simulations using the program AutoDock v4.2.3 with the default protocol in the screening of the virtual library [30]. The docking simulation was performed in quadruplicate, and the same substance was indicated as the first option in all simulations. Performance of this procedure ensured reproducibility of the results by avoiding false positives. The final model of *Zmays*CALDH bound to the best pose of the inhibitor was subjected to energy minimization (EM) by conjugate gradient (CG) using NAMD2 v2.8 software to correct potential unfavorable stereochemical clashes between protein and ligand as well as to adjust the active site to the presence of the ligand [31].

2.5. Redocking

It is assumed that the minimized final structure of *Zmays*CALDH bound to the inhibitor is the lowest energy conformation of the complex. So, redocking of the inhibitor was performed on the minimized complex to determine accurately the theoretical parameters K_i and $\Delta G_{binding}$.

2.6. Molecular dynamics

After identification and analysis of the putative inhibitor of *Zmays*CALDH, the stability of the complex formed was checked by molecular dynamics (MD) simulation techniques. Simulations of the protein in the apo form (*Zmays*CALDH-Apo) and that bound to the inhibitor (*Zmays*CALDH–DZN) were conducted separately on the monomeric structure. Additional studies were conducted on the tetrameric form of the enzyme bound to the inhibitor, to assess the stability of the biological unit (*Zmays*CALDHt), as well as interactions in the quaternary structure.

All MD simulations were performed under periodic boundary conditions using the NAMD2 package and CHARMM c35b2-c36a2 force fields [28,32]. The ligand structure was obtained directly from the Zinc database, and force field parameters were generated with the SwissParam tool [33]. Accurate partial charges for the ligand atoms were obtained by quantum calculation at B3LYP/6−311G level of theory with a standard solvation model implemented in Gaussian software [34]. The MD simulations were carried out in steps. First, the whole system was solvated in a cubic box whose dimensions were set at a minimum distance of 10 Å from the outer surface of the molecule. An appropriate amount of Na^+ was added to the system to neutralize its charge density. The whole system was then submitted to 50,000 EM steps by CG. The structure generated in this step was used in the redocking experiments. Next, the atoms of the protein and ligand were fixed in space, and the water and ions were subjected to 60 ps of MD. Again, the entire system was minimized by over 50,000 steps, and finally the whole system was equilibrated for 20 ns.

All simulations were conducted under constant conditions of the number of atoms, pressure and temperature (300 K, 1 atm) by using Langevin dynamics to control the kinetic energy of the system. Electrostatic interactions were calculated using the particle-mesh Ewald algorithm (PME) with a ratio of less than 1.0 Å between the grid points and the sizes of the primary factors. The radius of van der Waals interactions was 10 Å. The simulations were performed at 2-fs time intervals, and the integrals of the equations of motion and the coordinates were saved every 2 ps. All analyses were performed in the set of system configurations extracted at time intervals of 2 ps of simulation. The convergences of the different simulations were analyzed in terms of root mean square deviation (rmsd) over time and by the root mean square fluctuation (rmsf) of the last 2 ns (equilibration stage). The radius of gyration (r_{gyr}) was calculated to assess changes in enzyme compaction compared to the initial structure. All docking simulations were performed on an AMD Intel Core 2 Duo 2.60 GHz 2 GB machine, while MD simulations were performed on four nodes of an SGI Altix ICE 8400 LX consisting of two 3.33 GHz Intel Six Core 5680 units (48 cores) and 36 GB of RAM.

2.7. CALDH activity

Maize seeds were sanitized with 2 % sodium hypochlorite for 5 min, rinsed extensively with deionized water and dark-germinated at 25 °C on two sheets of moistened filter paper (Germitest, CEL 060). Twenty-five 3-day-old seedlings of uniform size were supported by an adjustable acrylic plate and dipped into a 10 × 16 cm glass container filled with 200 mL of nutrient solution, pH 6.0 [35]. The containers were kept in a growth chamber for 24 h at 25 °C, with a light/dark photoperiod of 12/12 h and a photon flux density of 280 μmol m^{-2} s^{-1}. *Zmays*CALDH was extracted as described by Nair et al. [16] with modifications. Fresh roots (3 g) were ground at 4 °C in 4.5 mL of extraction medium containing 50 mM Hepes-HCl (pH 8.0), 5 mM DTT, 1 mM EDTA, 10 % glycerol (v/v) and protease inhibitor cocktail (Sigma-Aldrich, P9599). The homogenate was centrifuged (2200 × *g*, 25 min, 4 °C), the supernatant was collected, and the protein extract was precipitated with 70 % saturation ammonium sulfate. After centrifugation (2200 × *g*, 15 min, 4 °C), the pellet was homogenized in extraction medium, and the sample was used as the enzyme preparation. DZN was dissolved in dimethyl sulfoxide (DMSO). For this, the control was performed with DMSO to avoid possible differences regarding this solvent.

For the *Zmays*CALDH activity assay, the reaction mixture contained 50 mM Hepes-HCl (pH 8.0), 1 mM NAD^+ and 100 μL of the partially purified enzyme preparation with or without 30 or 100 μM DZN, the enzymatic inhibitor. To protect the enzyme, the extraction medium contained 5 mM DTT, as a reducing agent, and protease inhibitors. All experiments were performed within a maximum of 30 min after obtaining the extract to keep the decrease in catalytic activity below 1 %. The mixture was incubated at 40 °C, and the reaction was initiated by addition of 2.5–100 μM coniferyl aldehyde, in a final volume of 1 mL. The reaction was stopped after 10 min by the addition of 60 μL of 3 M HCl. After centrifugation (16,000 × *g*, 2 min), the samples were filtered through a 0.45-μm disposable syringe filter (Hamilton® Co, Reno, Nevada, USA) and analyzed (20 μL) in a high-performance liquid chromatography (HPLC) system (Shimadzu® Prominence 20, Tokyo, Japan) equipped with a quaternary pump, an auto-sampler, a column oven and a diode-array detector. A reversed-phase Shim-pack® CLC-ODS column (150 mm × 4.6 mm, 5 μm) was used at 30 °C, together with an equivalent pre-column. The mobile phase was methanol:4 % acetic acid (30:70, v/v), with a flow rate of 1.0 mL min^{-1} for an isocratic run of 20 min. UV detection was carried out at 330 nm. Ferulic acid, *i.e.*, the product of the *Zmays*CALDH reaction, was identified by comparing its retention time with that of a standard compound. Protein was quantified by the Bradford method [36]. Parallel controls were made to eliminate any endogenous ferulic acid in the samples. *Zmays*CALDH activity was expressed as nmol ferulate h^{-1} mg^{-1} protein.

The maximal velocity values (V_{max}) and Michaelis–Menten constants (K_m) were obtained by fitting the Michaelis–Menten equation to the initial velocities (with or without DZN) using iterative nonlinear least-squares analysis (SigmaPlot 12.0, Systat Software, Inc., Chicago, IL, USA). Lineweaver–Burk plots were constructed to identify the inhibition type caused by DZN on *Zmays*CALDH.

3. Results and discussion

3.1. Homology modeling

The nucleotide sequence (NCBI EU969650.1) translated into amino acids showed 100 % identity (*e*-value 0.00) with a homolog protein noted as cytosolic ALDH RF2D (*Z. mays*) in UniProt (Q8S529) showing CALDH activity. This same sequence revealed the highest identity and an *e*-value of 0.00 with other plant ALDHs and coniferaldehyde/sinapaldehyde dehydrogenases. Thus, we have assumed that it corresponds to *Zmays*CALDH.

After identifying the sequence, the three-dimensional structure of the enzyme was modeled by homology. The sequence of *Zmays*CALDH showed 55.6 % identity with human mitochondrial ALDH2 (PDB ID: 3N80) solved at a resolution of 1.50 Å, enough for homology modeling [37,38]. For comparative purposes, the *Zmays*CALDH sequence followed the same initial numbering as the template. The final structure modeled was one of the four subunits that make up the biological unit of the enzyme, with 99.8 % of the residues in favorable regions of the Ramachandran plot, and only a single residue located in a region not allowed due to bias imported from the template, which it was not possible to correct in the modeling process. The structure of *Zmays*CALDH was modeled without NAD^+, because there is evidence that this

cofactor can produce steric conflicts in one of these conformations, which prevent the simultaneous binding of both NAD^+ and DZN in human ALDH [39]. However, some studies have shown that another conformation of NAD^+ does not result in clashes between DZN and NAD^+. These structural studies have shown that binding of NAD^+ to ALDH has great conformational flexibility [40,41]. This suggests that the coenzyme can show the necessary conformal flexibility to avoid steric conflicts, allowing the formation of a ternary enzyme–coenzyme–inhibitor complex [39]. The literature reports that kinetic inhibition analysis of DZN over human ALDH1 and ALDH2 shows that both enzymes perform competitive inhibition with the aldehyde and are uncompetitive with respect to NAD^+ [41,42]. As DZN inhibits ALDH isozymes by a competitive mechanism, this suggests that NAD^+ coenzyme may bind first to the catalytic site followed by aldehyde or DZN binding by a sequential ordered Bi–Bi mechanism [43].

DZN is the first isoflavone derivative known to inhibit human ALDH, and the first compound that inhibits, selectively and reversibly, ALDH2 at low concentrations. Most inhibitors of ALDH are irreversible, such as, for example, tetraethylthiuram disulfide (disulfiram®), an adjunctive therapeutic agent to chronic alcoholism [44]. Some structural studies on the ALDH2/DZN complex show that the loss of enzyme activity occurs by a rupture caused by DZN in the network of hydrogen bonds which stabilize the coenzyme binding sites and the catalytic site [39,45]. Binding of NAD^+ leads to a reordering of the coenzyme binding site, but only a partial rearrangement of the catalytic site. However, it is enough for DZN to exert its effect on the active site and, in consequence, to inhibit the enzyme.

3.2. Virtual screening

The library of compounds similar to the known inhibitors (Tanimoto index of 90 %) of human ALDH consists of 20 commercial compounds at the time of this research. Coniferyl aldehyde, the substrate of CALDH, was also included in the library for comparative purposes. The use of libraries containing compounds like known inhibitors of a given enzyme is a common strategy in drug discovery (focused, targeted libraries) [46], and may result in libraries with a small number of compounds. In addition, minor changes in the structure of a given compound (similar compound) may lead to more effective inhibition of a homologous enzyme. The virtual docking was carried out in quadruplicate, and in all simulations the flavonoid DZN (CID 107971; Fig. 1) revealed the best performance. DZN is a known inhibitor of human ALDH2 which catalyzes the oxidation of acetaldehyde to acetate [42,47]. In humans, it has been tested as a drug for the treatment of alcoholism and has been subjected to several biological tests [48,49].

Despite human ALDH and *Zmays*CALDH sharing the same mechanism of action, the discovery of DZN as an inhibitor of *Zmays*CALDH may not be a surprise. However, the fact that a compound inhibits human ALDH does not imply it automatically inhibits *Zmays*CALDH. These enzymes share structural differences which allow selective inhibition. As an example, we have earlier cited tetraethylthiuram disulfide (disulfiram®), a known inhibitor of human ALDH. However, this compound was not selected as an inhibitor of *Zmays*CALDH during our virtual screening, and so it was not tested herein due to its poor solubility in solvents non-toxic to plants.

Compared to the other inhibitors tested, DZN is the most soluble compound (partition coefficient of 0.77); it has been used as a drug in humans, and its adverse effects are well known [45,50]. Despite these promising aspects, in the docking procedure, the structure of the protein remained fixed while the ligand was flexible. So, it is possible that the binding site was not in the most favorable conformation for interaction with DZN. To correct this, the structure of the protein–ligand complex (*Zmays*CALDH–DZN) was minimized by CG and subjected to redocking analyses. The results are summarized in Table 1, and they reveal that minimization of the complex led to better interaction between the active site and ligand. This fact results in lower values of binding energy and K_i in the redocking when compared to the docking before minimization. After minimization of the complex, the value of $\Delta G_{binding}$ reflected the most accurate docking parameters and was used as a reference. In brief, the *in silico* findings herein suggest that *Zmays*CALDH has a higher affinity for DZN than ALDH2 itself.

Table 1
Theoretical binding parameters obtained by docking and redocking of DZN.

Target	Simulation	$\Delta G_{binding}$ (Kcal mol^{-1})	rmsd (Å)	K_i (μM)
*Zmays*CALDH	Docking	−8.72		0.409
*Zmays*CALDH-DZN	Redocking [a]	−9.29	1.80	0.156
*Hsapiens*ALDH2	Docking	−6.66		13.080
*Hsapiens*ALDH2-DZN (2vle)	Redocking	−8.76	0.83	0.379

[a] After energy minimization.

3.3. Molecular dynamics

To evaluate the stability of the modeled protein–ligand complex, and to gain more information about the contribution of each residue in stabilization of the ligand and in the contacts of the quaternary structure, we performed MD simulations of the monomer in 1) the apo form, 2) bound to DZN and 3) DZN linked to the tetrameric form at all four subunits. This form was chosen in the current work because, similarly, the structure of bovine and human ALDH2 has been described as a tetramer [39,51]. In studies with the monomeric form of *Zmays*CALDH docked with DZN, the best pose was minimized by 50,000 steps. On the other hand, the tetramer apo form had the ligand incorporated in each subunit by geometric docking, and then it was minimized by 50,000 steps. So, all structures were equilibrated as described in the Methods section. The equilibrium of the complex was obtained when the rmsd values of the main-chain atoms reached a plateau for at least 4 ns (Fig. 2). These results show that all complexes evaluated reached a thermodynamic equilibrium after 6 ns of simulation.

The r_{gyr} is defined as the root mean square of the collection of the distance of atoms about their common center of gravity. All complexes evaluated exhibited a constant r_{gyr} throughout the simulation time (Fig. 3). The results indicate that both the apo form and the complex maintained their original folding. It is noteworthy that the r_{gyr} and rmsd of the tetramer forms fluctuated less than those of the monomeric forms, suggesting that the tetramer is more stable than the monomeric form of *Zmays*CALDH. It reinforces the hypothesis that this is the likely biological unit of this enzyme as its template since *Zmays*CALDH has not yet been structurally characterized by experimental methods.

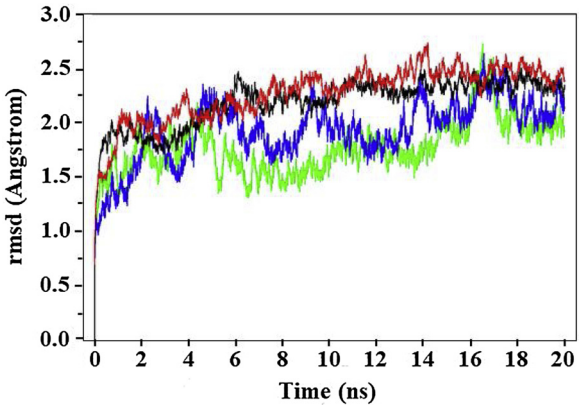

Fig. 2. Root mean square deviation (rmsd) behavior from the main chain atoms of *Zmays*CALDHt-Apo (black), *Zmays*CALDHt-DZN (red), *Zmays*CALDH-Apo (green), *Zmays*CALDH-DZN (blue) along simulation. (For interpretation of the references to colour in this figure legend, the reader is referred to the web version of this article).

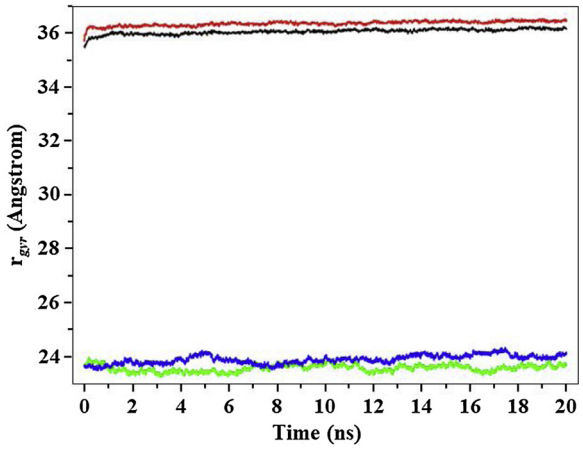

Fig. 3. Behavior of the radius of gyration (r_{gyr}) from *Zmays*CALDHt-Apo (black), *Zmays*CALDHt-DZN (red), *Zmays*CALDH-Apo (green), *Zmays*CALDH-DZN (blue) along simulation time. (For interpretation of the references to colour in this figure legend, the reader is referred to the web version of this article).

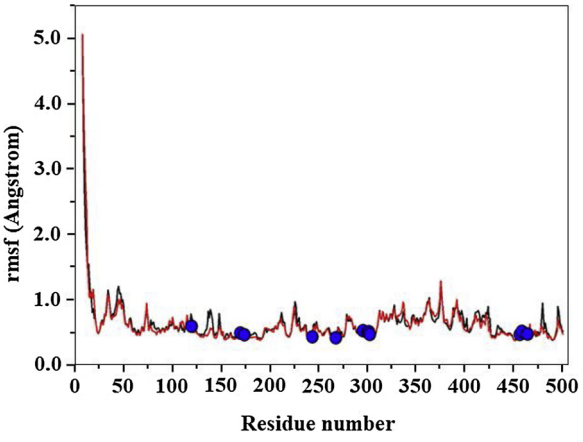

Fig. 4. Flexibility of the Cα atoms in the last 2 ns simulation calculated from the mean of the four subunits *Zmays*CALDHt-Apo (black), *Zmays*CALDHt-DZN (red). Residues of the active site had little positional variation during the equilibration period. The blue dots are the active site residues described in Table 2. (For interpretation of the references to colour in this figure legend, the reader is referred to the web version of this article).

Despite these results, the protein is not entirely static, and certain regions are more flexible than others. The flexibility of different regions in the monomer *Zmays*CALDH–DZN was identified through the rmsf of each residue, calculated from the Cα atoms throughout the last 2 ns of simulation, a period in which the complex was at equilibrium. The major fluctuations occurred in regions of the terminal residues of the protein (Fig. 4). The last 15 residues of the C-terminal form an anti-parallel β-sheet with residues 142–150, which were slightly affected by the fluctuation of the C-terminal region (Fig. 4). However, these regions of greater fluctuation did not affect the stabilization of residues in the active site (blue dots in Fig. 4).

3.4. Active site

There are two distinct sites in the structure of *Zmays*CALDH: one for the cofactor NAD^+ and the other for the substrate. Because the *Zmays*CALDH structure was modeled in the apo form, the location of the active site was taken from the description of human ALDH2 crystallized in the presence of DZN, and its spatial coordinates fed into the docking software [39]. In a crystal structure, description of the active site residues is made from the close contacts with the ligand. However,

Table 2
Contact frequency of residues in the active site of *Zmays*CALDH with DZN. Only residues with a frequency of contact greater than 5 % are shown. The residues in bold have more than 75 % of frequency of contact with ligand and define the active site in Fig. 4.

Residue	DZN contact Frequency	Residue	DZN contact frequency
ILE-119	**0.75**	**CYS-301**	**1.00**
ASP-120	0.24	**VAL-302**	**0.93**
PHE-169	**0.97**	LEU-426	0.25
MET-172	0.29	TYR-455	0.20
MET-173	**0.81**	**PHE-456**	**1.00**
THR-243	**0.82**	ALA-457	0.39
GLU-267	**1.00**	**PHE-458**	**0.96**
LEU-291	0.14	**PHE-464**	**0.95**
PHE-295	**0.98**	GLN-476	0.32
VAL-300	**0.84**		

this description is made with a static image that can hardly represent the dynamics of a protein in solution. It is also possible to identify the residues that comprise the active site, from their frequency of contact with the ligand. This information can be extracted from the trajectory of MD simulation. The advantage of MD regarding crystallography is identification of the residues with the highest frequency of contact that, consequently, would be the most important in anchoring the ligand. Table 2 shows the definition of the active site in *Zmays*CALDH, which was made from the residues that contacted DZN within a maximum distance of 4.0 Å. This result indicates that there is an increased frequency of contacts from hydrophobic residues with DZN, suggesting that this binding is stabilized essentially by van der Waals contacts.

This is most clear when one observes that Phe169 and Phe458 stabilize the ligand adhering to the DZN isoflavone, both residues being conserved in the model and template (Fig. 5). These results indicate that candidates for *Zmays*CALDH ligands must have a planar and non-polar structure. A striking feature of the ALDH2/DZN complex is the packing of the DZN planar isoflavone ring structure between layers of the plane of some residues' side chains (Fig. 5), wherein DZN is approximately 90 % buried. At the entrance of the active site of ALDH2, the glycoside group of DZN is anchored by H-bonds with the C═O of Asp457 and the NH— of Phe459. Binding of DZN did not cause any structural changes in this region, probably because these groups are inserted into the main chain of the protein, which reduces their degree of freedom [39].

A glycoside at position 7 (*O*-glycosidic bond) is essential for the inhibition of ALDH promoted by DZN, which explains why the aglycones genistein and daidzein inhibit ALDHs less than DZN [42]. Derivatives of 7-*O*-substituted daidzein are better inhibitors than daidzein [52]. The chemical properties of this active site provide an explanation for the affinities of many 7-*O*-substituted DZN compounds. So, DZN is bound between the catalytic and binding domains of NAD^+ [51,53]. These observations provide an explanation for both the affinity and specificity of ALDH2 with DZN (IC_{50} = 80 nM) and analogs with a different substituent at the glycoside position [39]. Analysis of the chemical topology of ALDH provides guidance for how the glucosyl group might be substituted with other groups to produce compounds with better pharmacokinetic properties while preserving the potency and specificity of DZN.

On the other hand, in the bottom of the cavity of the active site, Glu267 moves to make a charge–dipole contact at 3.1 Å with the OH4′ group of DZN. This contact takes place directly in *Zmays*CALDH and remains constant throughout all 20-ns simulations, different to that described for ALDH2, where this contact is mediated by a water molecule important for catalysis. This establishes a network of hydrogen bonds which stabilize the binding of compounds with the free OH4′ [39]. Studies regarding the ALDH2 structure–activity relationship indicate that this structural feature is important for ALDH2 inhibition,

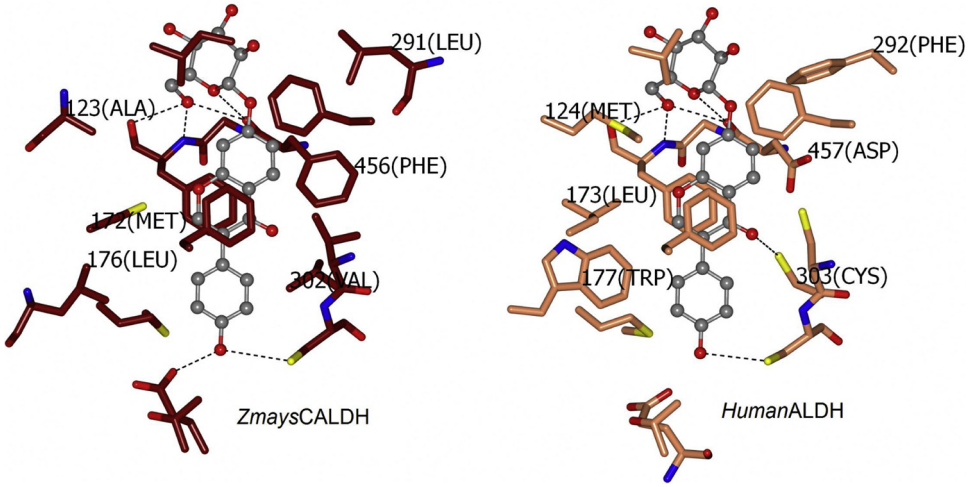

Fig. 5. Daidzin binding site at *Zmays*CALDH (brown) and ALDH2 crystallized with DZN. Dashed lines represent hydrogen bond between daidzin and protein residues. Labeled residues are differences among structures which allow selective inhibition.

and therefore we can extend this to *Zmays*CALDH inhibition [42,54,55]. The OH4′ group of DZN needs to be free and, thus, the steric environment around the OH4′ position excludes DZN analogs with a larger group substituted at this position, because our simulations indicate that this group makes a charge–dipole contact with the Glu267 of the active site.

Among the most evident changes in the active site of *Zmays*CALDH over ALDH2 lie the replacements Val120→Ile, Met124→Ala, Leu173→Met, Trp177→Leu, Phe292→Leu, Cys303→Val and Asp457→Phe456 (Fig. 5), which caused an increase in the volume from 225.8–264.2 Å^3 and in the surface area from 368.6–523.5 Å^2 in this cavity. Three residues (Ile119, Val302 and Phe456) from these substitutions have a high frequency of contact with DZN. This means that they are primarily responsible for the higher *in silico* affinity of CALDH for DZN compared to ALDH2. These three residues would also be key points for eventual design of a more selective inhibitor for *Zmays*CALDH.

3.5. Contacts of the quaternary structure

Evaluation of interfaces and intermolecular contacts of *Zmays*CALDH as well as of ALDH2 quaternary structures was performed using the PISA server at the European Bioinformatics Institute, and the results are summarized in Table 3. The $\Delta^i G$ indicates the free energy of solvation added by formation of the interface. The value is referred to as the difference between total energies of solvation of the structures isolated and interfaced. A negative $\Delta^i G$ corresponds to a hydrophobic interface or positive protein affinity. This does not include the contributions of hydrogen and salt bonds along the interface. $^iN_{res}$ indicates the average number of residues in the interface in the corresponding set. The parameters N_{HB} and N_{SB} indicate the numbers of potential hydrogen bonds and ionic interactions, respectively, along the interface [56].

3.6. Kinetic analysis

Using iterative, nonlinear, least-squares analysis to fit the Michaelis-Menten equation to initial velocities, non-linearized plots were created (Fig. 6A). The plots revealed the *Zmays*CALDH behavior in the presence of DZN, which clearly inhibited the enzyme. Compared to the control curve, initial velocities for the conversion of 2.5–100 μM coniferyl aldehyde to ferulate were reduced, on average, 36 % and 60 % when 30 and 100 μM DZN were added, respectively.

The inhibitory effects of DZN on *Zmays*CALDH activity were also apparent through analysis using linearized Lineweaver-Burk plots (Fig. 6B). V_{max} and K_m values determined with the method have been summarized in Table 4. K_m values determined for the *Zmays*CALDH enzyme were within the range of 7–12 μM at pH 8.8 and 26 °C, which had previously been determined for the CALDH enzyme from *Pseudomonas* sp. using coniferyl aldehyde as a substrate [57]. It was also close to values determined for ALDH1 (using acetaldehyde as substrate and DZN as inhibitor at pH 9.5), which were 12 μM (for hamsters) and 15 μM (for rats). However, the values differed from the K_m value previously determined for human ALDH1, which was 180 μM [52].

Similar values of V_{max} and different values for K_m (Table 4) produced a kinetic profile that was consistent with competitive inhibition, a finding that was supported by results using double-reciprocal plots (Fig. 6B). Therefore, these results have shown that the mechanism of inhibition of *Zmays*CALDH by DZN is competitive with respect to the coniferyl aldehyde substrate. The mechanism proposed herein was consistent with the mode of inhibition of human ALDH1 in relation to acetaldehyde and formaldehyde, which was supported in studies showing that DZN binds to the enzyme active site [42,52]. Consistent with the kinetic analysis, the 3D structure of the protein revealed that the predicted binding of DZN and substrate were mutually exclusive [42].

The experimental K_i value for *Zmays*CALDH (Table 4) was 14.1 μM and, therefore, close to those determined for human ALDH2 (20 μM) and ALDH1 (28 μM) [42,52]. One should also consider that the activity

Table 3
Interface comparisons of model and template structures.

Structure	Monomer to dimer interfaces A + B and C + D					Dimer to tetramer interfaces A to C and B to D				
	$^iN_{res}$	N_{HB}	N_{SB}	Interface area (Å^2)	$\Delta^i G$ (Kcal/mol)	$^iN_{res}$	N_{HB}	N_{SB}	Interface area (Å^2)	$\Delta^i G$ (Kcal/mol)
*Zmays*CALDH	78	34	8	2678	−25.8	46	20	6	1618	−9.4
3N80	77	51	8	2657	−25.1	45	26	10	1483	−3.6

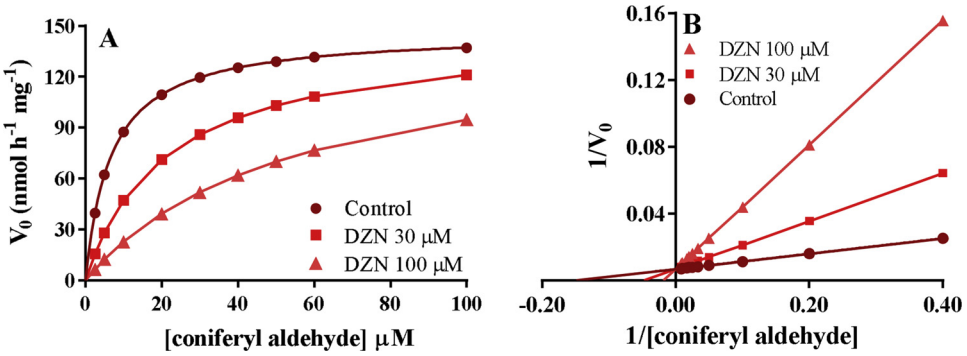

Fig. 6. Michaelis-Menten (A) and Lineweaver-Burk (B) plots indicating a kinetic profile consistent with competitive inhibition of *Zmays*CALDH by DZN. The enzyme activity was determined in reaction mixture without (●) or with 30 µM DZN (●), 100 µM DZN (●), and 2.5–100 µM coniferyl aldehyde for 10 min. The plots were obtained by fitting the Michaelis–Menten equation to the initial velocities using iterative nonlinear least-squares analysis.

Table 4
Kinetics parameters obtained by fitting the Michaelis-Menten equation to the initial velocities with or without DZN.

DZN (µM)	V_{max} (nmol h^{-1} mg protein^{-1})	K_m (µM)	K_i (µM)
0	146.4	6.7	
30	146.4	21.1	14.1
100	146.4	54.5	14.1

of *Zmays*CALDH was determined in a partially purified enzyme extract, whereas the purified protein was used for assays measuring ALDH2 activity with formaldehyde as substrate [42]. Moreover, the effect of DZN on *Zmays*CALDH has been evaluated for the first time herein and, therefore, no kinetic parameters have previously been reported in order to make direct comparisons between K_i values. Nonetheless, our findings regarding docking and kinetic analyses suggest that DZN can bind with more affinity to purified *Zmays*CALDH.

4. Conclusions

Summarizing, the results obtained *in silico* and *in vitro* provide a satisfactory degree of reliability with respect to the structure of *Zmays*CALDH modeled by homology and facilitated a virtual exploration of selective inhibitors of broad interest. As noted herein, DZN is an efficient and reversible competitive inhibitor of *Zmays*CALDH. So, it can be used to study the role of this enzyme in the phenylpropanoid pathway as well as the structural role of ferulic acid in cell-wall architecture, and properties of lignocellulosic biomass. The computational approach applied in the current work proved to be an effective tool for the discovery of new inhibitors of *Zmays*CALDH, and the findings can be extended to other enzymes related to biotechnological applications. The conclusive results shown here contribute to new perspectives for developing alternative methods to genetic modification for silencing the enzymes of the phenylpropanoid pathway in this plant. As a future perspective, applying DZN in growth and digestibility of maize in field experiments could add new information and strengthen the evidence revealed herein. It is our next challenge.

Declaration of Competing Interest

The authors declare that there are no conflicts of interest.

Acknowledgements

This work was supported by the National Council for Scientific and Technological Development (CNPq) [grant number 477075/2011-8], Araucaria Foundation [grant number 20133960], and in part by the Coordenação de Aperfeiçoamento de Pessoal de Nível Superior - Brasil (CAPES) - Finance Code 001. O. Ferrarese-Filho and R. Marchiosi are researcher fellows of CNPq. The authors also acknowledge the National Center for High Performance Processing (CENAPAD/SP, Brazil) for providing computational facilities.

References

[1] P.E. Marriott, L.D. Gómez, S.J. McQueen-Mason, Unlocking the potential of lignocellulosic biomass through plant science, New Phytol. 209 (2016) 1366–1381, https://doi.org/10.1111/nph.13684.
[2] R. Van Acker, A. Déjardin, S. Desmet, L. Hoengenaert, R. Vanholme, K. Morreel, F. Laurans, H. Kim, N. Santoro, C. Foster, G. Goeminne, F. Legee, C. Lapierre, G. Pilate, J. Ralph, W.A. Boerjan, Different metabolic routes for coniferaldehyde and sinapaldehyde with cinnamyl alcohol dehydrogenase1 deficiency, Plant Physiol. 175 (2017) 1018–1039, https://doi.org/10.1104/pp.17.00834.
[3] J.H. Grabber, J. Ralph, C. Lapierre, Genetic and molecular basis of grass cell-wall degradability. I. Lignin-cell wall matrix interactions, C. R. Biol. 327 (2004) 455–465.
[4] W.R. de Souza, P.K. Martins, J. Freeman, T.K. Pellny, L.V. Michaelson, B.L. Sampaio, F. Vinecky, A.P. Ribeiro, B.A.D.B. da Cunha, A.K. Kobayashi, P.A. de Oliveira, R.B. Campanha, T.F. Pacheco, D.C.I. Martarello, R. Marchiosi, O. Ferrarese-Filho, W.D. dos Santos, R. Tramontina, F.M. Squina, D.C. Centeno, M. Gaspar, M.R. Braga, M.A.S. Tiné, J. Ralph, R.A.C. Mitchell, H.B.C. Molinari, Suppression of a single BAHD gene in *Setaria viridis* causes large, stable decreases in cell wall feruloylation and increases biomass digestibility, New Phytol. 218 (2018) 81–93, https://doi.org/10.1111/nph.14970.
[5] D.M. de Oliveira, A. Finger-Teixeira, T.R. Mota, V.H. Salvador, F.C. Moreira-Vilar, H.B.C. Molinari, R.A.C. Mitchell, R. Marchiosi, O. Ferrarese-Filho, W.D. dos Santos, Ferulic acid: a key component in grass lignocellulose recalcitrance to hydrolysis, Plant Biotechnol. J. 13 (2015) 1224–1232, https://doi.org/10.1111/pbi.12292.
[6] C. Álvarez, F.M. Reyes-Sosa, B. Díez, Enzymatic hydrolysis of biomass from wood, Microb. Biotechnol. 9 (2016) 149–156, https://doi.org/10.1111/1751-7915.12346.
[7] T. Umezawa, Lignin modification in planta for valorization, Phytochem. Rev. (2018), https://doi.org/10.1007/s11101-017-9545-x.
[8] U.C. Kalluri, H. Yin, X. Yang, B.H. Davison, Systems and synthetic biology approaches to alter plant cell walls and reduce biomass recalcitrance, Plant Biotechnol. J. 12 (2014) 1207–1216, https://doi.org/10.1111/pbi.12283.
[9] A. Eudes, Y. Liang, P. Mitra, D. Loqué, Lignin bioengineering, Curr. Opin. Biotechnol. 26 (2014) 189–198, https://doi.org/10.1016/j.copbio.2014.01.002.
[10] R. Van Acker, R. Vanholme, V. Storme, J.C. Mortimer, P. Dupree, W. Boerjan, Lignin biosynthesis perturbations affect secondary cell wall composition and saccharification yield in Arabidopsis thaliana, Biotechnol. Biofuels 6 (2013), https://doi.org/10.1186/1754-6834-6-46.
[11] N.D. Bonawitz, C. Chapple, Can genetic engineering of lignin deposition be accomplished without an unacceptable yield penalty? Curr. Opin. Biotechnol. 24 (2013) 336–343, https://doi.org/10.1016/j.copbio.2012.11.004.
[12] M.J. Meents, Y. Watanabe, A.L. Samuels, The cell biology of secondary cell wall biosynthesis, Ann. Bot. 121 (2018) 1107–1125, https://doi.org/10.1093/aob/mcy005.
[13] R. Vanholme, I. Cesarino, K. Rataj, Y. Xiao, L. Sundin, G. Goeminne, H. Kim, J. Cross, K. Morreel, P. Araujo, L. Welsh, J. Haustraete, C. McClellan, B. Vanholme, J. Ralph, G.G. Simpson, C. Halpin, W. Boerjan, Caffeoyl shikimate esterase (CSE) is an enzyme in the lignin biosynthetic pathway in Arabidopsis, Science 341 (2013) 1103–1106, https://doi.org/10.1126/science.1241602.
[14] C.J. Liu, Y. Cai, X. Zhang, M. Gou, H. Yang, Tailoring lignin biosynthesis for efficient and sustainable biofuel production, Plant Biotechnol. J. 12 (2014) 1154–1162, https://doi.org/10.1111/pbi.12250.
[15] J. Barros, H. Serk, I. Granlund, E. Pesquet, The cell biology of lignification in higher plants, Ann. Bot. 115 (2015) 1053–1074, https://doi.org/10.1093/aob/mcv046.
[16] R.B. Nair, The *Arabidopsis thaliana* reduced epidermal fluorescence1 gene encodes an aldehyde dehydrogenase involved in ferulic acid and sinapic acid biosynthesis, Plant Cell 16 (2004) 544–554, https://doi.org/10.1105/tpc.017509.
[17] W.D. dos Santos, M.L.L. Ferrarese, C.V. Nakamura, K.S.M. Mourão, C.A. Mangolin, O. Ferrarese-Filho, Soybean (*Glycine max*) root lignification induced by ferulic acid. The possible mode of action, J. Chem. Ecol. 34 (2008) 1230–1241, https://doi.org/10.1007/s10886-008-9522-3.
[18] G.A. Bubna, R.B. Lima, D.Y.L. Zanardo, W.D. dos Santos, M.L.L. Ferrarese, O. Ferrarese-Filho, Exogenous caffeic acid inhibits the growth and enhances the lignification of the roots of soybean (*Glycine max*), J. Plant Physiol. 168 (2011)

1627–1633, https://doi.org/10.1016/j.jplph.2011.03.005.
[19] A.R. Soares, R.C. Siqueira-Soares, V.H. Salvador, M.L.L. Ferrarese, O. Ferrarese-Filho, The effects of L-DOPA on root growth, lignification and enzyme activity in soybean seedlings, Acta Physiol. Plant. 34 (2012), https://doi.org/10.1007/s11738-012-0979-x.
[20] E. Gasteiger, A. Gattiker, C. Hoogland, I. Ivanyi, R.D. Appel, A. Bairoch, ExPASy: The proteomics server for in-depth protein knowledge and analysis, Nucleic Acids Res. 31 (2003) 3784–3788, https://doi.org/10.1093/nar/gkg563.
[21] E.M. Zdobnov, R. Apweiler, InterProScan - an integration platform for the signature-recognition methods in InterPro, Bioinformatics 17 (2001) 847–848, https://doi.org/10.1093/bioinformatics/17.9.847.
[22] A. Lobley, M.I. Sadowski, D.T. Jones, pGenTHREADER and pDomTHREADER: new methods for improved protein fold recognition and superfamily discrimination, Bioinformatics 25 (2009) 1761–1767, https://doi.org/10.1093/bioinformatics/btp302.
[23] A. Eswar, N. Webb, B. Marti-Renom, M.A. Madhusudhan, M.S. Eramian, D. Shen, M.Y. Pieper, U. Sali, Comparative protein structure modeling using modeller, Curr. Protoc. Bioinf. 5 (2006) 5.6.
[24] The CCP4 suite: programs for protein crystallography, Acta Crystallogr. Sect. D Biol. Crystallogr. 50 (1994) 760–763, https://doi.org/10.1107/S0907444994003112.
[25] T. Liu, Y. Lin, X. Wen, R.N. Jorissen, M.K. Gilson, BindingDB: A web-accessible database of experimentally determined protein-ligand binding affinities, Nucleic Acids Res. 35 (2007) 198–201, https://doi.org/10.1093/nar/gkl999.
[26] E.E. Bolton, Y. Wang, P.A. Thiessen, S.H. Bryant, PubChem: Integrated Platform of small molecules and biological activities, Annu. Rep. Comput. Chem. 4 (2008) 217–241, https://doi.org/10.1016/S1574-1400(08)00012-1.
[27] C. Knox, V. Law, T. Jewison, P. Liu, S. Ly, A. Frolkis, A. Pon, K. Banco, C. Mak, V. Neveu, Y. Djoumbou, R. Eisner, A.C. Guo, D.S. Wishart, DrugBank 3.0: a comprehensive resource for "Omics" research on drugs, Nucleic Acids Res. 39 (2011) 1035–1041, https://doi.org/10.1093/nar/gkq1126.
[28] A. Gaulton, L.J. Bellis, A.P. Bento, J. Chambers, M. Davies, A. Hersey, Y. Light, S. McGlinchey, D. Michalovich, B. Al-Lazikani, J.P. Overington, ChEMBL: A large-scale bioactivity database for drug discovery, Nucleic Acids Res. 40 (2012) 1100–1107, https://doi.org/10.1093/nar/gkr777.
[29] J.J. Irwin, T. Sterling, M.M. Mysinger, E.S. Bolstad, R.G. Coleman, ZINC: A free tool to discover chemistry for biology, J. Chem. Inf. Model. 52 (2012) 1757–1768, https://doi.org/10.1021/ci3001277.
[30] G.M. Morris, R. Huey, W. Lindstrom, M.F. Sanner, R.K. Belew, D.S. Goodsell, A.J. Olson, AutoDock4 and AutoDockTools4: Automated docking with selective receptor flexibility, J. Comput. Chem. 30 (2009) 2785–2791, https://doi.org/10.1002/jcc.21256.AutoDock4.
[31] J.C. Phillips, R. Braun, W. Wang, J. Gumbart, E. Tajkhorshid, E. Villa, C. Chipot, R.D. Skeel, L. Kalé, K. Schulten, Scalable molecular dynamics with NAMD, J. Comput. Chem. 26 (2005) 1781–1802, https://doi.org/10.1002/jcc.20289.
[32] A.D. Mackerell, M. Feig, C.L. Brooks, Extending the treatment of backbone energetics in protein force fields: limitations of gas-phase quantum mechanics in reproducing protein conformational distributions in molecular dynamics simulation, J. Comput. Chem. 25 (2004) 1400–1415, https://doi.org/10.1002/jcc.20065.
[33] V. Zoete, M.A. Cuendet, A. Grosdidier, O. Michielin, SwissParam: a fast force field generation tool for small organic molecules, J. Comput. Chem. 32 (2011) 2359–2368.
[34] M.J. Frisch, G.W. Trucks, H.B. Schlegel, G.E. Scuseria, M.A. Robb, J.R. Cheeseman, G. Scalmani, V. Barone, B. Mennucci, G.A. Petersson, H. Nakatsuji, M. Caricato, X. Li, H.P. Hratchian, A.F. Izmaylov, J. Bloino, G. Zheng, J.L. Sonnenberg, M. Had, Gaussian 9, Revision A.01, Gaussian, Inc., Wallingford CT, 2009.
[35] J. Dong, F. Wu, G. Zhang, Influence of cadmium on antioxidant capacity and four microelement concentrations in tomato seedlings (*Lycopersicon esculentum*), Chemosphere 64 (2006) 1659–1666, https://doi.org/10.1016/j.chemosphere.2006.01.030.
[36] M.M. Bradford, A rapid and sensitive method for the quantitation of microgram quantities of protein utilizing the principle of protein-dye binding, Anal. Biochem. 72 (1976) 248–254, https://doi.org/10.1016/0003-2697(76)90527-3.
[37] B. Rost, Twilight zone of protein sequence alignments, Protein Eng. 12 (1999) 85–94.
[38] A.S. Yang, B. Honig, An integrated approach to the analysis and modeling of protein sequences and structures. III. A comparative study of sequence conservation in protein structural families using multiple structural alignments, J. Mol. Biol. 301 (2000) 691–711, https://doi.org/10.1006/jmbi.2000.3975.
[39] E.D. Lowe, G.-Y. Gao, L.N. Johnson, W.M. Keung, Structure of daidzin, a naturally occurring anti-alcohol-addiction agent in complex with mitochondrial aldehyde dehydrogenase, J. Med. Chem. 51 (2008) 4482–4487.
[40] P.K. Hammen, A. Allali-Hassani, K. Hallenga, T.D. Hurley, H. Weiner, Multiple conformations of NAD and NADH when bound to human cytosolic and mitochondrial aldehyde dehydrogenase, Biochemistry 41 (2002) 7156–7168, https://doi.org/10.1021/bi012197t.
[41] S.J. Perez-Miller, T.D. Hurley, Coenzyme isomerization is integral to catalysis in aldehyde dehydrogenase, Biochemistry 42 (2003) 7100–7109, https://doi.org/10.1021/bi034182w.
[42] W.M. Keung, B.L. Vallee, Daidzin: a potent, selective inhibitor of human mitochondrial aldehyde dehydrogenase, Proc. Natl. Acad. Sci. 90 (1993) 1247–1251, https://doi.org/10.1073/pnas.90.4.1247.
[43] R.C. Vallari, R. Pietruszko, Kinetic mechanism of the human cytoplasmic aldehyde dehydrogenase E1, Arch. Biochem. Biophys. 212 (2012) 9–19, https://doi.org/10.1016/0003-9861(81)90338-6.
[44] R.C. Vallari, R. Pietruszko, Human aldehyde dehydrogenase: mechanism of inhibition of disulfiram, Science 216 (1982) 637–639, https://doi.org/10.1126/science.7071604.
[45] G.Y. Gao, D.J. Li, W.M. Keung, Synthesis of daidzin analogues as potential agents for alcohol abuse, Bioorg. Med. Chem. Lett. 11 (2003) 4069–4081, https://doi.org/10.1016/S0968-0896(03)00397-3.
[46] W.M. Keung, O. Lazo, L. Kunze, B.L. Vallee, Daidzin suppresses ethanol consumption by Syrian golden hamsters without blocking acetaldehyde metabolism, Proc. Natl. Acad. Sci. 92 (1995) 8990–8993.
[47] W.P. Walters, M.T. Stahl, M.A. Murcko, Virtual screening - an overview, Drug Discov. Today 3 (1998) 160–178.
[48] V.M. Keung, V.L. Vallee, Daidzin and daidzein supress free-choice ethanol intake by Syrian golden hamsters, Proc. Natl. Acad. Sci. 90 (1993) 10008–10012.
[49] Y. Wang, J. Xiao, T.O. Suzek, J. Zhang, J. Wang, Z. Zhou, L. Han, K. Karapetyan, S. Dracheva, B.A. Shoemaker, E. Bolton, A. Gindulyte, S.H. Bryant, PubChem's BioAssay database, Nucleic Acids Res. 40 (2012) D400–412, https://doi.org/10.1093/nar/gkr1132.
[50] D.H. Kim, H.A. Jung, S.J. Park, J.M. Kim, S. Lee, J.S. Choi, J.H. Cheong, K.H. Ko, J.H. Ryu, The effects of daidzin and its aglycon, daidzein, on the scopolamine induced memory impairment in male mice, Arch. Pharm. Res. 33 (2010) 1685–1690, https://doi.org/10.1007/s12272-010-1019-2.
[51] C.G. Steinmetz, P. Xie, H. Weiner, T.D. Hurley, Structure of mitochondrial aldehyde dehydrogenase: the genetic component of ethanol aversion, Structure 5 (1997) 701–711, https://doi.org/10.1016/S0969-2126(97)00224-4.
[52] W.M. Keung, A.A. Klyosov, B.L. Vallee, Daidzin inhibits mitochondrial aldehyde dehydrogenase and suppresses ethanol intake of Syrian golden hamsters, Proc. Natl. Acad. Sci. 94 (1997) 1675–1679, https://doi.org/10.1073/pnas.94.5.1675.
[53] L. Ni, J. Zhou, H. Weiner, T.D. Hurley, Human liver mitochondrial aldehyde dehydrogenase: three-dimensional structure and the restoration of solubility and activity of chimeric forms, Protein Sci. 8 (2009) 2784–2790, https://doi.org/10.1110/ps.8.12.2784.
[54] N. Rooke, D.J. Li, J. Li, W.M. Keung, The mitochondrial monoamine oxidase-aldehyde dehydrogenase pathway: a potential site of action of daidzin, J. Med. Chem. 43 (2000) 4169–4179, https://doi.org/10.1021/jm990614i.
[55] G.Y. Gao, D.J. Li, W.M. Keung, Synthesis of potential antidipsotropic isoflavones: inhibitors of the mitochondrial monoamine oxidase - aldehyde dehydrogenase pathway, J. Med. Chem. 44 (2001) 3320–3328, https://doi.org/10.1021/jm0101390.
[56] E. Krissinel, K. Henrick, Inference of macromolecular assemblies from crystalline state, J. Mol. Biol. 372 (2007) 774–797, https://doi.org/10.1016/j.jmb.2007.05.022.
[57] S. Achterholt, H. Priefert, A. Steinbüchel, Purification and characterization of the coniferyl aldehyde dehydrogenase from *Pseudomonas sp*. Strain HR199 and molecular characterization of the gene, J. Bacteriol. 180 (1998) 4387–4391.